Available online at www.sciencedirect.com
ScienceDirect
Journal of the European Ceramic Society 29 (2009) 497–503
www.elsevier.com/locate/jeurceramsoc

Low-cost preparation and frictional behaviour of a three-dimensional needled carbon/silicon carbide composite

Yanzhi Cai, Yongdong Xu *, Bin Li, Shangwu Fan, Litong Zhang, Laifei Cheng, Lin Yu

National Key Laboratory of Thermostructure Composite Materials, Northwestern Polytechnical University, Xi'an Shaanxi 710072, PR China

Received 28 February 2008; received in revised form 21 June 2008; accepted 23 June 2008

Abstract

A low-cost carbon/silicon carbide (C/SiC) composite was manufactured by phenolic resin impregnation–pyrolysis combined with liquid silicon infiltration. The carbon fiber preform was prepared by three-dimensional needling. A carbon/carbon composite with a density of 1.22 g/cm^3 after only one impregnation–pyrolysis cycle was achieved by using hot-pressing curing. The density of the final C/SiC was 2.10 g/cm^3 with a porosity of 4.50% and SiC-content of 45.73%. The C/SiC composite had a high thermal conductivity of 48.72 W/(m K) perpendicular to the friction surface and demonstrated good friction and wear properties. The static and average dynamic friction coefficients were 0.68 and 0.32 (at a braking velocity of 28 m/s). The weight wear rates of the rotating disk and stationary disk were respectively 7.71 and 5.60 mg/cycle with linear wear rates, 1.67 and 1.22 μm/cycle, at a braking velocity of 28 m/s.

Keywords: Hot-pressing; Composite; Thermal conductivity; Wear resistance; SiC

1. Introduction

Carbon fiber reinforced silicon carbide (C/SiC) composites have received considerable attention for braking applications because of their excellent friction behaviour and oxidation resistance.[1–3] The conventional braking materials are metallic materials which have some limitations such as high density, poor performance at high temperature and poor corrosion resistance.[4] Subsequently, C/C composite brakes were developed to fulfill a significant reduction of weight, high performance and long lifetime. However, C/C brakes suffer from their insufficient stability of the coefficient of friction (COF) caused by humidity, temperature. Furthermore, the fiber and matrix in carbon composites will degrade above 450 °C in oxidative conditions, leading to the failure of brake. The C/SiC composites have advantages of lower sensibility to service environments over C/C composites. The SiC matrix can improve the wear resistance and has high thermal conductivity (TC) and good oxidation resistance as well as thermal shock resistance.[5–7] Additionally, the friction data indicate that they have the potential to offer stable COF.[8] Hence, C/SiC brake disks are not only ready for the application in high-performance cars and emergency brake systems, but also for the application in the new generation materials of aircraft brake.[9]

In the early 1990s, Krenkel et al.[1] had investigated the C/SiC composites for high-performance automobile applications. Short fiber reinforcement in combination with pressing technique followed by liquid silicon infiltration (LSI) was employed to manufacture C/SiC composites. However, as the lack of fibers perpendicular to the friction surface, the unstable COF lay in the too high friction surface temperature as a result of the low TC perpendicular to the friction surface. The coating on the surface could be employed to improve the TC perpendicular to the friction surface,[1,10] but the thickness of coating was limited, and the difference of C/SiC substrate and coating material in the coefficient of thermal expansion (CTE) leaded to more or less microcracked surface. Fan et al.[11] prepared high-performance C/SiC brakes by chemical vapor infiltration (CVI) combined with LSI, using the infiltration of a carbonaceous gas into the carbon fiber preform, but the rate of deposition was very slow. Four brake companies in the US: Aircraft Braking System, Goodrich, Honeywell and Parker-Hannifin, jointly carried out the investigation by polymer impregnation pyrolysis (PIP).[9] In this process, decomposition and volume shrinkage of organic precursor during pyrolysis resulted in a large number

* Corresponding author. Tel.: +86 29 88494619; fax: +86 29 88494620.
E-mail address: ydxu07@gmail.com (Y. Xu).

0955-2219/$ – see front matter © 2008 Elsevier Ltd. All rights reserved.
doi:10.1016/j.jeurceramsoc.2008.06.021

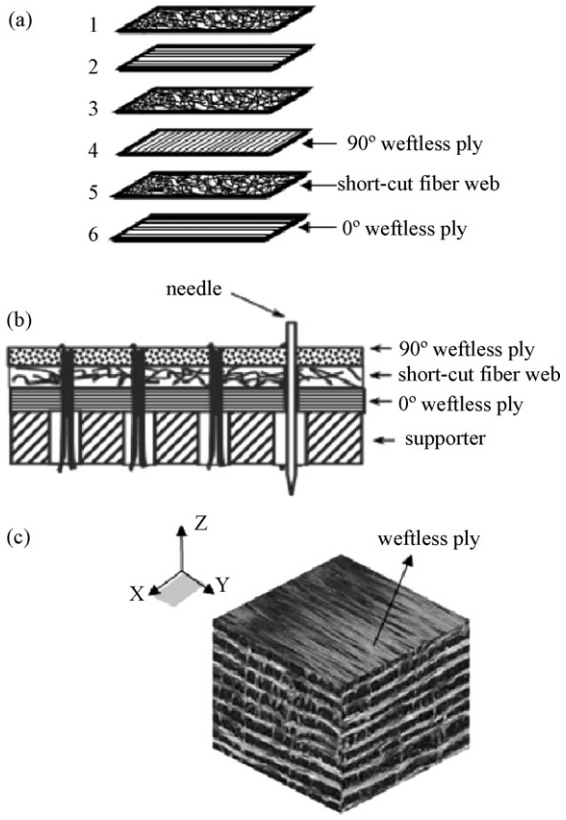

Fig. 1. (a) The position of weftless ply and short-cut fiber web; (b) the detailed view of a Z-fiber bundle generated during the needling process; (c) structure of 3D needled preform.

of microcracks and pores in the matrix, requiring the repeated impregnation and pyrolysis cycles to increase the density. Therefore, it is necessary to develop a more efficient technique for fabricating the high-performance C/SiC composite braking material.

In this study, a short-time and low-cost process for three-dimensional (3D) needled C/SiC composites was proposed. The microstructures and frictional behaviour were investigated.

2. Experimental procedures

2.1. Sample preparation

The C/SiC composite was prepared by the combination of PIP and LSI, and hot-pressing curing was employed during PIP. The 3D needled integrated felt (Fig. 1) with a density of 0.55 g/cm^3 was used as the preform. It was fabricated by repeatedly overlapping the layers of 0° weftless ply, short-cut fiber web and 90° weftless ply with needle-punching step by step. All the carbon fiber types were polyacrylonitrile (PAN)-based carbon fiber (T 700, 12 K tow, Toray, Japan). The fiber volume contents of the weftless plies, the webs and the needled fibers were 24.0, 4.5 and 1.5%, respectively.

As mentioned above, the C/SiC composites were prepared with two steps. The first one was the PIP process to manufacture the porous C/C composite. The preform was placed in an air-pressure impregnation device (Northwestern Polytechnical University, Xi'an, PR China) and impregnated with the resin under unidirectional pressure and then isostatic pressure. The impregnation pressure was 0.4–0.6 MPa and impregnation time was 1.5–2 h. The as-impregnated preform was cured under hot-pressing at a maximum temperature of 180 °C and a maximum pressure of 30 MPa. The prepared carbon fiber reinforced polymer (CFRP) was pyrolyzed at 900 °C. Sequentially, high-temperature treatment (HTT) at 2000 °C was performed to get a C/C composite with a adequate density. The manufacturing scheme of this C/C composite is shown in Fig. 2. Finally, the LSI process was used to prepare the C/SiC composite. The LSI was conducted at the range of 1450–1700 °C for 1–3 h under vacuum.

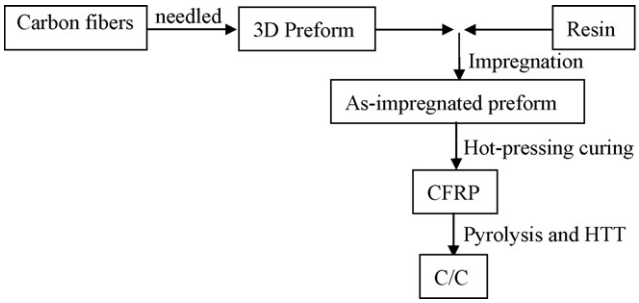

Fig. 2. Manufacturing scheme of type A C/C.

The composites prepared with the above method were named as type A, while the composites derived from four resin impregnation, curing (without using hot-pressing) and pyrolysis cycles were named as type B as comparison.

2.2. Braking tests

The tests of friction and wear properties of C/SiC samples were operated on MM-1000 testing machine, which was described previously in detail.[11] The tests were carried out with one rotating disk of Ø 76 mm × Ø 52 mm × 8 mm (76 mm in outer diameter, 52 mm in inner diameter and 8 mm in thickness) pressed against one stationary disk of Ø 90 mm × Ø 55 mm × 8 mm. The braking conditions for friction and wear performance tests are shown in Table 1. During braking tests, some parameters such as rotating speed n (r/min), braking torque M (N m), surface temperature of brake disks T (°C), and braking time t (s) were automatically recorded. The friction performance was also conducted in static conditions. The tests were repeated

Table 1
Braking conditions for friction and wear performance tests[a]

Braking velocity		Braking times
Linear velocity (m/s)	Rotational velocity (r/min)	
5	1440	30
10	2880	20
15	4320	20
20	5760	20
25	7200	10
28	8064	10

[a] The inertia and braking pressure were 0.235 kg m^2 and 0.3 MPa.

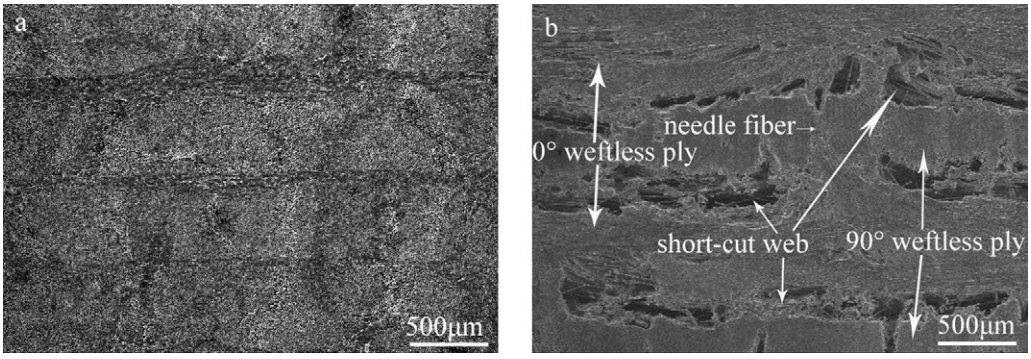

Fig. 3. SEM micrographs of (a) type A and (b) type B CFRP.

for 10 times in static conditions. The COF could be calculated from the following equation:

$$M = \frac{\mu\,(r_1 + r_2)\,P}{2} \quad (1)$$

where M is the braking torque, μ the COF, P the braking pressure, r_1 the inner radius, and r_2 is the outer radius. The friction stability coefficient S was calculated according to the following equation:

$$S = \frac{\mu_{cp}}{\mu_{max}} \quad (2)$$

where μ_{cp} is the average COF and μ_{max} is the maximum COF.

The wear performance was evaluated with weight wear and linear wear. The weight or linear wear rate was calculated with the weight difference or thickness difference of the sample before and after braking tests divided by braking times.

2.3. Characterization of TC

The TC perpendicular to the friction surfaces were tested at room temperature through Ø 100 mm × 8 mm samples on a thermal constant analyser (Hot Disk TPS-2500, Sweden). The test method is based on the use of a transiently heated plane sensor. The Hot Disk sensor consists of an electrically conducting pattern in the shape of a double spiral. This spiral is sandwiched between two thin insulating sheets.

When performing the TC measurement the plane Hot Disk sensor was fitted between two pieces of the sample—each one with a plane surface facing the sensor. By passing an electrical current high enough to increase the temperature of the sensor between a fraction of a degree up to several degrees, the temperature increase as a function of time was recorded at the same time. The temperature increase of the sample was dependent on the power delivered to the sample surfaces facing the sensors. The time-dependent temperature increase was given as the following equation:

$$\Delta T_{ave}(\tau) = \frac{P_0}{\pi^{3/2} r \Lambda} D(\tau) \quad (3)$$

where $\Delta T_{ave}(\tau)$ is the temperature increase of the sample surface on the other side of the insulating layer and facing the Hot Disk sensor, P_0 the total output of power from the sensor, r the overall radius of the Disk, Λ the TC of the sample being tested, and $D(\tau)$ is a dimensionless time-dependent function. So, the temperature increase could be expressed as a linear function of $D(\tau)$. From the slope of this straight line the TC could be calculated.

2.4. Microstructure and phase analysis

The open porosity and bulk density of samples were measured by Archimedes' method. The microstructures were investigated by scanning electron microscope (SEM, S-4200, Hitachi, Japan). The gravimetric analysis[12] was employed to determine the mass contents of C, Si, and SiC in the composites. The residual Si was removed by dissolving the composite in a mixture of hydrofluoric and nitric acid (HNO_3:HF = 4:1) at 40 °C for 48 h, whereas the content of C was measured by burning it off at 700 °C for 20 h in air, so the SiC-content could be calculated.

3. Results and discussion

3.1. Microstructure characterization during preparation process

Fig. 3 shows micrographs of the CFRP. As shown in Fig. 3(a), the CFRP of type A was very dense, attaining a density of 1.44 g/cm^3 after a one-shot impregnation and showing almost no macropores. In contrast, the CFRP of type B (Fig. 3(b)), which only attained a density of 1.29 g/cm^3 after four times of impregnation, had a lot of macropores in both the inter-bundles and inter-plies regions. SEM investigations show an effective impregnation of the carbon fiber cloths in this low-cost route. The dense matrix of type A was due to resin further filling into pores and fiber volume content increasing during hot-pressing curing.

The density of type A C/C was 1.22 g/cm^3, which was similar to that of type B C/C (1.19 g/cm^3), despite only one impregnation and pyrolysis cycle being performed. It is noted that the fiber volume fraction increase of 67% (from 30 to 50 vol.%) was achieved in type A C/C using hot-pressing curing. The needled fibers, conducing greatly to liquid Si infiltrating into C/C, should have been increased in the volume fraction with a similar proportion. Furthermore, needled fibers in type A C/C curved around to propagate between laminas (Fig. 4(a)) by hot-pressing whereas those in type B C/C were mainly perpendicular to the lamina direction (Fig. 4(b)). The curved needled fibers were favorable

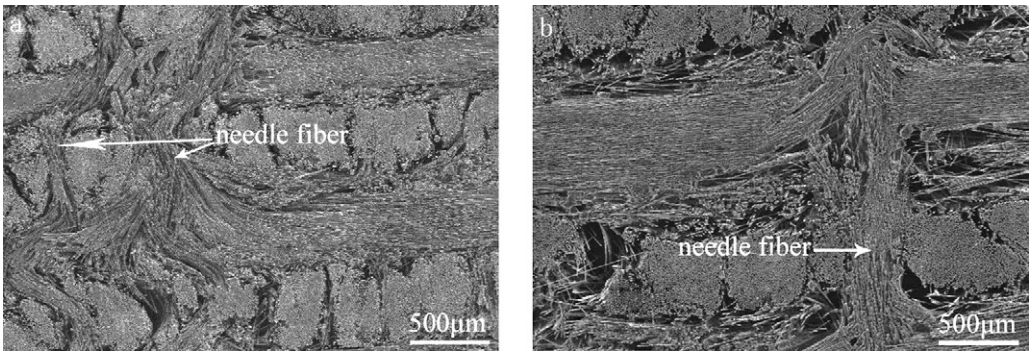

Fig. 4. SEM micrographs of needle fibers in (a) type A and (b) type B C/C.

greatly for molten Si filling in the initial pores within inter-plies, because the shape of infiltration channels was changed from the right-angle into arc.

Therefore, much Si was absorbed and a large amount of SiC matrix was formed in the C/SiC of type A. A few isolated macropores ranging from 20 to 300 μm were retained in both the inter-bundles and inter-plies regions (Fig. 5(a)). But for the C/SiC of type B, less Si was absorbed and the size of pores, especially of those within inter-plies, was much larger (Fig. 5(b)). With a further observation of the intra-bundle of type A C/SiC, the dense inter-fibers carbon matrix could be identified, some residual micropores which were hardly accessible to Si were detected (Fig. 5(c)). Only areas of inter-bundles, inter-plies and needled fibers were sparse fiber regions, where pores acted as infiltration channels of Si melt with high capillary forces, leading to a severer siliconization there (the grey regions in Fig. 5(a)). Accordingly, the dense carbon fibers inside the fiber bundles were effectively protected from the reaction with Si, a layer of SiC together with residual Si resulted around the bundles (Fig. 5(c)). Thus, only a small amount of load-bearing carbon fibers were converted into SiC. The composite with such kind of structural features is also named as C/C–SiC composite.

3.2. Phase compositions and physical properties

The phase compositions and physical properties of C/SiC composites are listed in Table 2. The SiC produced in type A C/SiC was obviously higher than that in type B C/SiC. Likewise, the density of type A C/SiC was much higher and its porosity was accordingly much lower. The measured TC perpendicular to the friction surface, 48.72 W/(m K), was also significantly higher than that of type B C/SiC, 27.05 W/(m K).

It has been well known that the higher the SiC-content, the higher the TC is expected to be. Moreover, the TC also depends on the fiber architecture. A small amount of fiber content, especially of needled fiber content, and the large inter-plies pores can

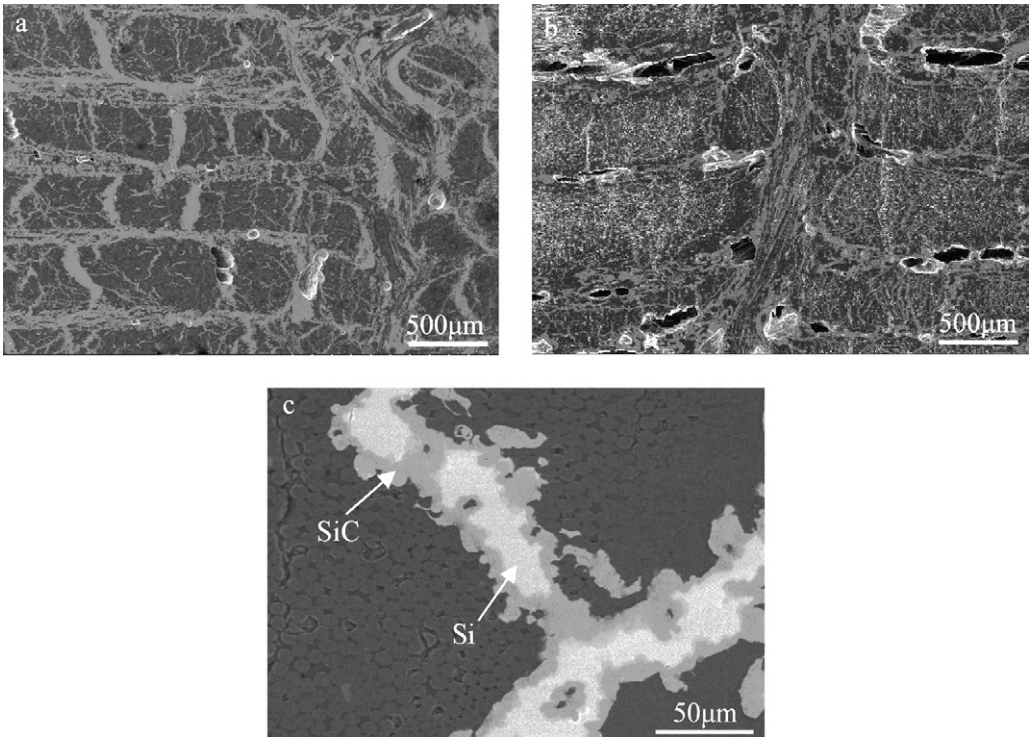

Fig. 5. SEM micrographs of (a) type A and (b) type B C/SiC, (c) backscattered electron image of intra-bundles and inter-bundles of (a).

Table 2
Phase compositions and physical properties of C/SiC composites

Type	Constitutes (%)			Density (g/cm^3)	Open porosity (%)	TC (W/(m K))
	C	SiC	Si			
A	43.44	45.73	10.83	2.100	4.500	48.72
B	51.78	35.38	12.84	1.900	13.64	27.05

contribute to the low TC perpendicular to the friction surface.[13] Type A C/SiC possessed a higher TC due to a higher SiC-content matrix, a higher fiber volume fraction as well as fewer and lesser inter-plies pores. Increasing SiC-content within the composite is a cost-efficient way to improve the TC, but a higher Si uptake and subsequently a higher SiC formation have to sacrifice the fiber volume content as a rule.[1,10] However, hot-pressing curing employed in the present work could increase the contents of both SiC and fiber volume and decreased the porosity, which was able to increase the TC greatly.

3.3. Braking behaviour

3.3.1. Friction properties

Dynamic friction properties of C/SiC composites are shown in Fig. 6. The variation curves of COF under different braking velocities of type A C/SiC (Fig. 6(a)) were all in the shape of inverse echelon. The braking began at a certain sliding velocity and ended with a standstill, the COF increased with decreasing velocity, reaching the highest value just before the end of braking.

The higher the COF, the higher the braking efficiency. The more stable the COF, the higher the efficiency of the brake control system. The stability of friction curve, however, decreased gradually with increasing braking velocities, and vibratory phenomena was aggravated. What was more, lower and lower COF at the beginning of braking resulted from higher temperature of friction surface due to higher energy input.[1,10] The product pv which is proportional to the areal braking performance P/A_f (performance density) is responsible for the value of the COF:

$$\frac{P}{A_f} = \mu p v \tag{4}$$

where P is the braking performance (W), p the pressure (MPa), v the braking velocity (m/s), A_f the friction area (m^2), and μ is the COF. In the present work, pressure was fixed (0.3 MPa), the higher velocity produced the higher performance density (A_f was regarded as a constant), resulting in the higher temperature on the friction surface.

The COF remains stable up to a critical ratio of P/A_f. Once P/A_f exceeding this critical ratio, the C/SiC tribo-system is never able to sustain high braking properties because the material overheats locally by so-called hot spots. As a result, the COF decreases while the surface temperature increases further. The higher the critical ratio is possessed by materials, the easier the stability is sustained under higher energy braking conditions. There are several ways to improve the critical ratio of P/A_f. High TC perpendicular to the friction surfaces which results in the high heat flux transferred from the outer friction surfaces to the centers of the disks in time is one of the ways. The average COF and friction stability coefficient of type A disks at a braking velocity of 28 m/s were 0.32 and 0.42 (Fig. 6(b)), which was acceptable.

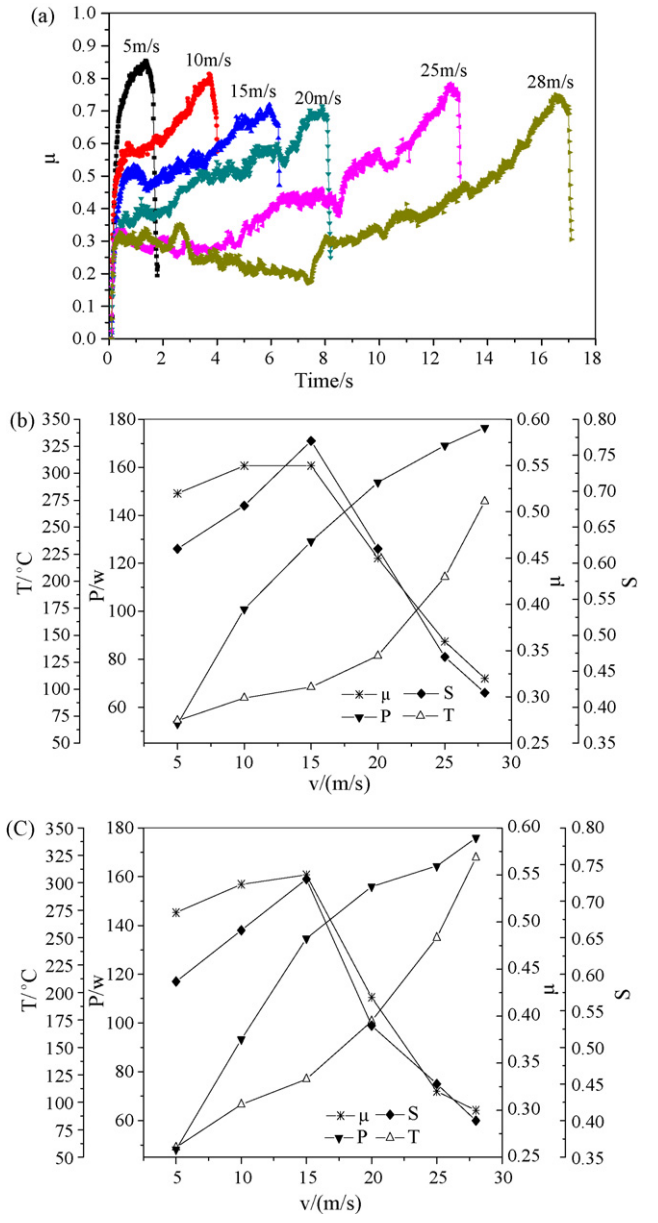

Fig. 6. (a) COF curves of type A C/SiC at different linear velocities of 5, 10, 15, 20, 25 and 28 m/s; effects of linear velocities on braking properties of (b) type A and (c) type B C/SiC including COF μ, friction stability coefficient S, braking performance P and friction surface temperature T.

Despite the small sizes of both type disks (only 8 mm in thickness), the surface temperature of type A disks was lower than that of type B disks at the same braking conditions, especially when the braking velocity exceeding 15 m/s, the differences reached 40–50 °C (Fig. 6(b) and (c)). Both the COF and friction stability coefficient of type A C/SiC were slightly higher than those of type B C/SiC at the same braking conditions.

It is noted that the static COF (0.68) was much higher than the average dynamic COF at any braking velocities for type A C/SiC composite. The value was also higher than that (0.52) of type B C/SiC composite and as much again of that (0.34) of C/SiC composite prepared by CVI combined with LSI.[11] If static COF is high enough, brake can keep aircraft resting on the ground after its engine starts running before accelerating and preparing to take off, which can reduce the aircraft gliding distance before takeoff.

3.3.2. Wear resistance

The wear rates of C/SiC disks including the rotating disks and stationary disks during braking tests are shown in Fig. 7. The materials showed an increasing tendency in the wear rates with increasing braking velocities. At the same braking conditions, both the weight and linear wear rates of stationary disks were lower than those of rotating disks; both the weight and linear wear rates of type A disks (Fig. 7(a)) were lower than those of type B disks (Fig. 7(b)). At a braking velocity of 28 m/s, the weight wear rates of type A disks were 7.71 and 5.60 mg/cycle with linear wear rates, 1.67 and 1.22 μm/cycle; the weight wear rates of type B disks were 14.16 and 8.50 mg/cycle with linear wear rates, 2.18 and 1.42 μm/cycle.

The heat is transmitted from the outer friction surface to the center of the material in time by higher TC perpendicular to the friction surface, which reduces thermal stress. Wear resistance is improved by higher SiC-content, since SiC has higher hardness, melting point, abradability and oxidation resistance.[10] Moreover, the material with lower porosity has lower linear wear and oxidation abrasion rates because of the reduced channels for oxygen entering. All these resulted in the much more

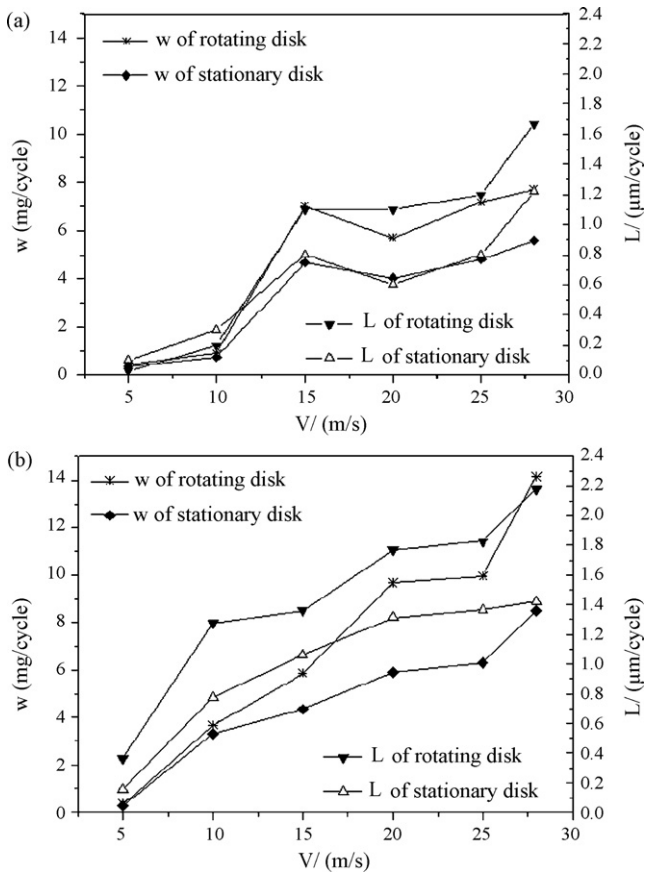

Fig. 7. Effects of linear velocities on wear behaviour of (a) type A and (b) type B C/SiC (w: weight wear rate; L: linear wear rate).

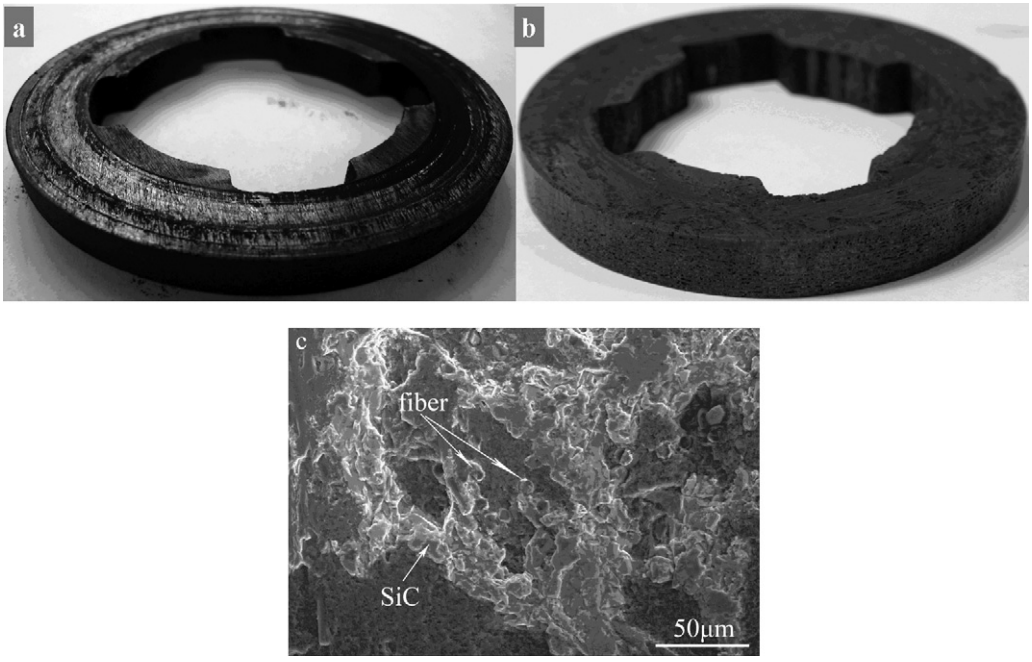

Fig. 8. Friction surface qualities of C/SiC disks: (a) type A and (b) type B rotating disks; (c) micro-peaks in the friction surface.

excellent wear resistance of type A than that of type B C/SiC composite.

3.3.3. Friction surface morphology

The wear-induced surfaces are significantly determined by the abrasion and damage mechanism between the contact surfaces, which results in the variation of the COF. The COF is determined by several factors other than the friction surface temperature, such as the mechanical deformation of the contact junction, the ploughing effect of wear debris, the true area of solid contact and the adhesion between the contact surfaces. The surface qualities of C/SiC disks including type A disk and type B disk are shown in Fig. 8. Their true contact areas approached the nominal areas and the widths of outside-annuluses and inside-annuluses on the surfaces were nearly zero (Fig. 8(a) and (b)), which improved the COF and friction stability coefficients.

The wear surface of type A disk displayed circumferential grooves in the direction of slide, whereas that of type B disk exhibited many macropores derived from the large inter-plies pores. There were a large amount of micro-peaks or micro-valleys in the brake disk surfaces, and these micro-peaks were mainly composed of SiC and fibers extruded through the friction surface which were all hard (Fig. 8(c)). These micro-peaks meshed with micro-valleys, leading to shearing, deformation, breaking, fall-off and becoming to wear debris (Fig. 8(a)) under the braking energy. At the same time, some grooves (Fig. 8(a)) were left as a result of broken micro-peaks ploughing on the friction surfaces.[11] The broken micro-peaks were easy to fill in macropores in the friction surface of type B disks, which prevented the ploughing effect.

Ploughing effect resulted in high friction resistance; grooves in the friction surface meshed with micro-peaks, increasing the true area of solid contact and leading to shearing during slide, both factors improved the COF of type A disks. The macropores in the friction surfaces of type B disks improved the COF similar to grooves but increased oxidation abrasion because of their acting as channels for oxygen entering.

4. Conclusions

(1) Hot-pressing curing in the PIP combined with LSI is a short-time and low-cost approach to fabricate a C/SiC composite.
(2) The carbon/carbon composite with a density of 1.22 g/cm^3 after one impregnation–pyrolysis cycle and the increase in volume content of carbon fibers by 67% was obtained. The density of the final C/SiC was 2.10 g/cm^3 with a porosity of 4.50% and SiC-content of 45.73%.
(3) The C/SiC composite had a high TC of 48.72 W/(m K) perpendicular to the friction surface.
(4) The C/SiC composite demonstrated good friction performance as well as wear resistance. The static and average dynamic COF were 0.68 and 0.32 (at a braking velocity of 28 m/s). The weight wear rates of the rotating disk and stationary disk were respectively 7.71 and 5.60 mg/cycle with linear wear rates, 1.67 and 1.22 μm/cycle, at a braking velocity of 28 m/s.

Acknowledgements

The authors acknowledge the financial supports of Natural Science Foundation of China (Contract No. NSFC50672076), Program for Changjiang Scholars and Innovative Research Team in University.

References

1. Krenkel, W., Heidenreich, B. and Renz, R., C/C–SiC composites for advanced friction systems. *Adv. Eng. Mater.*, 2002, **4**(7), 427–436.
2. Gadow, R. and Speicher, M., CMC brake disks in serial production-the competition between cost effectiveness and technical performance. *Ceram. Eng. Sci. Proc.*, 2002, **23**(4), 115–123.
3. Xu, Y. D., Zhang, Y. N., Cheng, L. F., Zhang, L. T., Lou, J. J. and Zhang, J. Z., Preparation and friction behavior of carbon fiber reinforced silicon carbide matrix composites. *Ceram. Int.*, 2007, **33**, 439–445.
4. Haug, T. and Rebstock, K., New material technologies for brakes. In *Advanced Brake Technology*, *vol. 4*, ed. B. Breuer and U. Dausend. SAE International, USA, 2003, pp. 256–260.
5. Krenkel, W., Cost effective processing of composites by melt infiltration (LSI-Process). *Ceram. Eng. Sci. Proc.*, 2001, **22**, 442–444.
6. Mei, H., Cheng, L. F., Zhang, L. T. and Xu, Y. D., Modeling the effects of thermal and mechanical load cycling on a C/SiC composite in oxygen/argon mixtures. *Carbon*, 2007, **45**, 2195–2204.
7. Odeshi, A. G., Mucha, H. and Wielage, B., Manufacture and characterization of a low cost carbon fibre reinforced C/SiC dual matrix composite. *Carbon*, 2006, **44**, 1994–2001.
8. Paris, J.-Y., Vincent, L. and Denape, J., High-speed tribological behaviour of a carbon/silicon carbide composite. *Comp. Sci. Technol.*, 2001, **61**, 417–423.
9. Vaidyaraman, S., Purdy, M., Walker, T. and Horst, S., C/SiC material evaluation for aircraft brake applications. In *High Temperature Ceramic Matrix Composites: 4th International Conference on High Temperature Ceramic Matrix Composites (HT-CMC4) Proceedings*, ed. S. Munich, 2001, pp. 802–808.
10. Krenkel, W., C/C–SiC composites for hot structures and advanced friction systems. *Ceram. Eng. Sci. Proc.*, 2003, **24**(4), 583–592.
11. Fang, S. W., Zhang, L. T., Xu, Y. D., Cheng, L. F., Lou, J. J., Zhang, J. Z. *et al.*, Microstructure and properties of 3D needle-punched carbon/silicon carbide brake materials. *Comp. Sci. Technol.*, 2007, **67**, 2390–2398.
12. Frieβ, M., Krenkel, W., Brandt, R. and Neuer, G., Influence of process parameters on the thermophysical properties of C/C–SiC. In *High Temperature Ceramic Matrix Composites*, *vol. 4*, ed. S. Weinheim. Wiley-VCH Press, 2001, pp. 328–333.
13. Tang, S. F., Deng, J. Y., Wang, S. J. and Liu, W. C., Fabrication and characterization of C/SiC composites with large thickness, high density and near-stoichiometric matrix by heaterless chemical vapor infiltration. *Mater. Sci. Eng. A*, 2007, **465**, 290–294.